ELSEVIER

Contents lists available at ScienceDirect

# Organic Geochemistry

journal homepage: www.elsevier.com/locate/orggeochem





# Identifying the drivers of GDGT distributions in alkaline soil profiles within the Serengeti ecosystem

Mark D. Peaple <sup>a,\*</sup>, Emily J. Beverly <sup>b</sup>, Brittany Garza <sup>b</sup>, Samantha Baker <sup>b</sup>, Naomi E. Levin <sup>c</sup>, Jessica E. Tierney <sup>d</sup>, Christoph Häggi <sup>a,1</sup>, Sarah J. Feakins <sup>a</sup>

- \* Department of Barth Sciences, University of Southern California, Los Angeles, CA, USA
- b Department of Barth and Atmospheric Sciences, University of Houston, TX, USA
- <sup>c</sup> Department of Earth and Environmental Sciences, University of Michigan, MI, USA
- Department of Geosciences, University of Arisona, Tucson, AZ, USA

## ARTICLE INFO

#### Associate Editor-Stefan Schouten

Keywords: Soil profile Serengeti GDGT Carbon isotope Temperature

#### ABSTRACT

Surface soil glycerol dialkyl glycerol tetraether (GDGT) distributions are influenced by mean annual air temperature as well as soil pH. However, the controls on GDGT distributions with depth in soil profiles are less wellknown. We report a study of soil profiles in warm, carbonate-precipitating, alkali soils in the Serengeti ecosystem, Tanzania. Measurements of temperature, pH, salinity, and complementary data available from carbonates and organics from the same soil pits provide an interpretive framework for the observed patterns in branched (br-) and isoprenoidal (iso-) GDGTs in soil profiles. While brGDGT distributions at the soil surface primarily reflect mean annual temperature, a warm bias at depth indicates additional sub-surface controls on brGDGT distributions. We consider whether degradation or in situ production in response to alkaline pH and salinity also modulate brGDGTs. We find that the Archaeol Caldarchaeol Ecometric (ACE) index correlates with soil salinity, which both increase with depth. These results support in situ microbial production in deeper soil settings, with pH and salinity controlling the microbial community composition. We also compared brGDGTpredicted mean annual air temperatures (MAAT) to published clumped isotope thermometry on carbonates in the same soils and found that the median temperatures of both proxies were the same at 23 °C. We suggest further comparison of proxy performance in carbonate-bearing soils and geological archives. Differences in the nature of the proxy recorders may broaden sample availability for paleothermometry and help to identify confounding factors in each proxy system.

## 1. Introduction

Branched glycerol dialkyl glycerol tetraether (brGDGTs) are membrane lipids composed of a branched alkyl chain with 4 to 6 methyl groups (De Jonge et al., 2014a) which are produced by bacteria and are found in a variety of environments including soils, peats, lakes, and coastal marine environments. However, the identity of the bacteria which produce brGDGTs is still mostly unknown (Weijers et al., 2006, 2009; Sinninghe Damsté et al., 2011, 2014, 2018).

Branched glycerol dialkyl glycerol tetraether (brGDGTs) lipids have been shown to be reliable recorders of temperature in modern surface soils and peats (Weijers et al., 2007; De Jonge et al., 2014b; Naafs et al., 2017; Dearing Crampton-Flood et al., 2020). This is likely due to bacteria changing the degree of methylation of membrane lipids under different temperature conditions in order to adjust the rigidity of their membranes (Weijers et al., 2007; Naafs et al., 2021). Whilst much progress has been made on how different environmental variables (e.g., temperatures, pH and soil moisture content) affect the distributions of brGDGTs in surface soils (e.g., Peterse et al., 2009; Huguet et al., 2010; Dirghangi et al., 2013; Menges et al., 2014; Dang et al., 2016), our knowledge of brGDGTs in deeper soils (> 0.1 m) is limited (Davtian et al., 2016). Interpretations of controlling factors can be divided into two classes: temporal (i.e., to what extent does modern production contribute to deep soil brGDGTs) and environmental (how would chemical conditions deeper in a soil affect brGDGTs). In surface soils, <sup>13</sup>C-labelling studies have shown turnover of brGDGTs on the timescales

<sup>\*</sup> Corresponding author.

E-mail address: peaple@usc.edu (M.D. Peaple).

Current address: Department of Earth Sciences, ETH Zurich, Switzerland.

of decades (Weijers et al., 2010; Huguet et al., 2017). In deeper soil horizons, compound specific radiocarbon analyses of brGDGTs have yielded mean turnover times of 1400 5900 years in mid-latitude soils which is a slower turnover rate compared to most other particulate organic carbon components (Gies et al., 2021).

Although surface soils have been the focus of most brGDGT calibration efforts (De Jonge et al., 2014b; Naafs et al., 2017; Dearing Crampton-Flood et al., 2020), understanding the processes that control brGDGT distributions at depth, including the transfer of extractable GDGTs to a non-extractable pool, organo-metallic complexations in Podzols, growth depth and post-depositional effects on GDGT distributions (Huguet et al., 2010; Zech et al., 2012; Yamamoto et al., 2016) is important when applying brGDGT proxies in paleosols and loess-paleosol sequences (Peterse et al., 2014) for both paleoclimate and paleoaltimetry studies (Coffinet et al., 2017; Bai et al., 2018; Li et al., 2018; Feng et al., 2019) where the deeper soils are often all that are preserved (Cleveland et al., 2007; Tabor and Myers, 2015; Beverly et al., 2018).

In addition to the brGDGTs that have been relatively well-studied in global surface soils, isoprenoidal GDGTs (isoGDGTs) produced by archaea are abundant in dryland alkali surface soils (Yang et al., 2014; H. Wang et al., 2017), and thus might be useful for diagnosing paleo soil moisture content (Xie et al., 2012; Yang et al., 2014). IsoGDGTs are composed of two C<sub>40</sub> isoprenoid chain with a number of cyclopentane and cyclohexane rings connected by ether bonds to two terminal glycerol groups (Li et al., 2016). Here, we measure the distribution of both brGDGTs and isoGDGTs at multiple soil sites and depths across a precipitation gradient in the Serengeti grassland. The 5-methyl brGDGT index (MBT 5Me) correlates with MAAT of soils on both global (De Jonge et al., 2014b) and local scales (Yang et al., 2015). MBT 5Me is similar to the methylation (MBT ) index  $_{\mbox{\scriptsize except}}$  that MBT  $_{\mbox{\scriptsize 5Me}}$  excludes 6-methyl brGDGTs and consequently shows a stronger relationship with MAAT (De Jonge et al., 2014b). We derived brGDGT temperature estimates using a global soil calibration of the MBT 5Me index to MAAT (Dearing Crampton-Flood et al., 2020). We then compared the known MAAT (Fick and Hijmans, 2017) between surface samples (0.1 m) and deeper samples (0.1 1.6 m), to determine if deeper soil samples are dominated by: (1) modern brGDGT production reflective of surface environmental conditions, (2) modern production reflecting deep soil environmental conditions or (3) by fossil brGDGTs reflecting past surface or deep soil conditions. In order to discriminate between these options, we evaluated changes in GDGT concentrations and compare to a suite of complementary environmental and biomarker information including temperature, pH, salinity and organic (biomarker) concentrations. We also calculated predicted soil pH based on CBT (De Jonge et al., 2014b) and compare this to measured soil pH in both surface and subsurface samples.

Additionally, these soil profiles have already been studied for clumped isotopes (Beverly et al., 2021) allowing us to compare the carbonate and organic paleothermometers. Clumped isotope thermometry records the formation temperature of carbonate and is based on the abundance of the doubly substituted isotopologue <sup>13</sup>C<sup>18</sup>O<sup>16</sup>O (reported as 47), which is proportional to the temperature-dependent ordering of <sup>13</sup>C and <sup>18</sup>O in carbonate minerals (Ghosh et al., 2006; Schauble et al., 2006). Both brGDGT and clumped isotope thermometry have been calibrated in modern environments (Kelson et al., 2017, 2020; Dearing Crampton-Flood et al., 2020) and are relatively stable over geological time (Finnegan et al., 2011; Kemp et al., 2014). However, to our knowledge, these proxies have not been directly compared at the same site. Comparison in the same soil profiles allows us to constrain how each proxy responds to the same environmental conditions. We use these modern soil profile observations to offer suggestions to guide future use of these proxies in paleoenvironmental studies.

#### 2. Study location and climate

The Serengeti ecosystem spans 30,000 km² in Tanzania and Kenya, in eastern Africa. A transect of 11 sites was used to study the soils in the region (34 36 E, 1 2 S, 1153 1667 m above sea level; Fig. 1). Mean annual air temperatures (MAAT) at these sites vary from 19.2 to 22.8 C and mean annual precipitation (MAP) ranges from 499 to 846 mm (Table 1; Fick and Hijmans, 2017). There are two rainy seasons: March to May and October to November (Norton-Griffiths et al., 1975). The vegetation is mostly grassland plains, dissected by riverine forest and woodlands based on Landsat remote sensing and ground-truthing in 1998 2002 (Reed et al., 2009) and correspond to observed conditions in 2018 when samples were collected. Most sites are grasslands ( 10% woody cover), except for three locations (Banagi, 80 100% shrubs; Kemarishe and Makoma; 20 50% tree canopy cover).

With some exceptions (e.g., Anderson et al., 2014; Perez-Angel et al., 2020), most global soil calibrations have been performed in the absence of detailed soil temperature logging, and thus soils are calibrated to MAAT obtained from global temperature products. Similarly, we obtain MAAT from WorldClim2 (Fick and Hijmans, 2017), which has a regional (eastern Africa) average temperature RMSE of 0.75 C and a spatial resolution of 1 km. In these Serengeti soils, we additionally have in situ measurements of temperatures in soil profiles at four sites (Ndabaka, Musabi, Kemarishe and Naabi Hill) using nine HOBO 64 K Pendant® temperature loggers (accuracy of 0.53 C) buried at depths ranging from 20 to 150 cm (Beverly et al., 2021) between 22/02/2018 to 26/01/2019.

#### 3. Materials and methods

#### 3.1. Soil sampling

Soil samples were collected during February 2018, as part of a prior study of soil carbonates (Beverly et al., 2021). Soil profiles (n 11) were studied by digging soil pits until refusal (up to 160 cm), often to indurated petrocalcic horizons. Soils were classified in the field according to USDA soil order descriptors and comprise of Inceptisols (n 4), Alfisol (n 1) and Mollisols (n 6). Carbonates were present below 40 cm at all but two sites and these nodules were sampled and studied for clumped isotopes as reported in Beverly et al. (2021).

Samples for laboratory pH analyses were collected at all sites at 10 cm resolution. Samples for biomarker analyses were collected from the top 10 cm of soil (below the litter layer), in the middle of the profiles at  $\sim 60$  cm, and in the deepest sector of the profiles at around 100–160 cm. Each sample averages three sub-samples from the 1.5 m width of the soil pit. The soil samples designated for organic analyses were previously studied for total organic carbon concentration (TOC), bulk carbon isotopic composition, as well as plant wax n-alkane and n-alkanoic acid concentrations and isotopes (Zhang et al., 2021). Here we use the neutral polar fraction, purified from the total lipid extracts in the same soil samples, to study the GDGTs.

## 3.2. Soil properties

Soil pH, electrical conductivity (EC), and total dissolved solids (TDS) were measured at the University of Houston using a Hanna Instruments HI 9813 6 m. Prior to measurements the meter was equilibrated to ambient temperature, pH was calibrated using Hanna Instruments buffer solution HI7007 (pH 7.01) and EC/TDS were calibrated using EC calibration solution HI 70,442 (1.41 mS/cm). TDS was determined by conversion from EC within the instrument and thus TDS range is dependent upon the calibration of EC. A slurry of each soil with distilled water (1:2, v/v) was stirred vigorously to break up any soil particle aggregates. The pH, EC, and TDS were measured after 15 min to allow the solution to equilibrate and particulate matter to settle. The methodology is similar to that of Weijers et al. (2007).

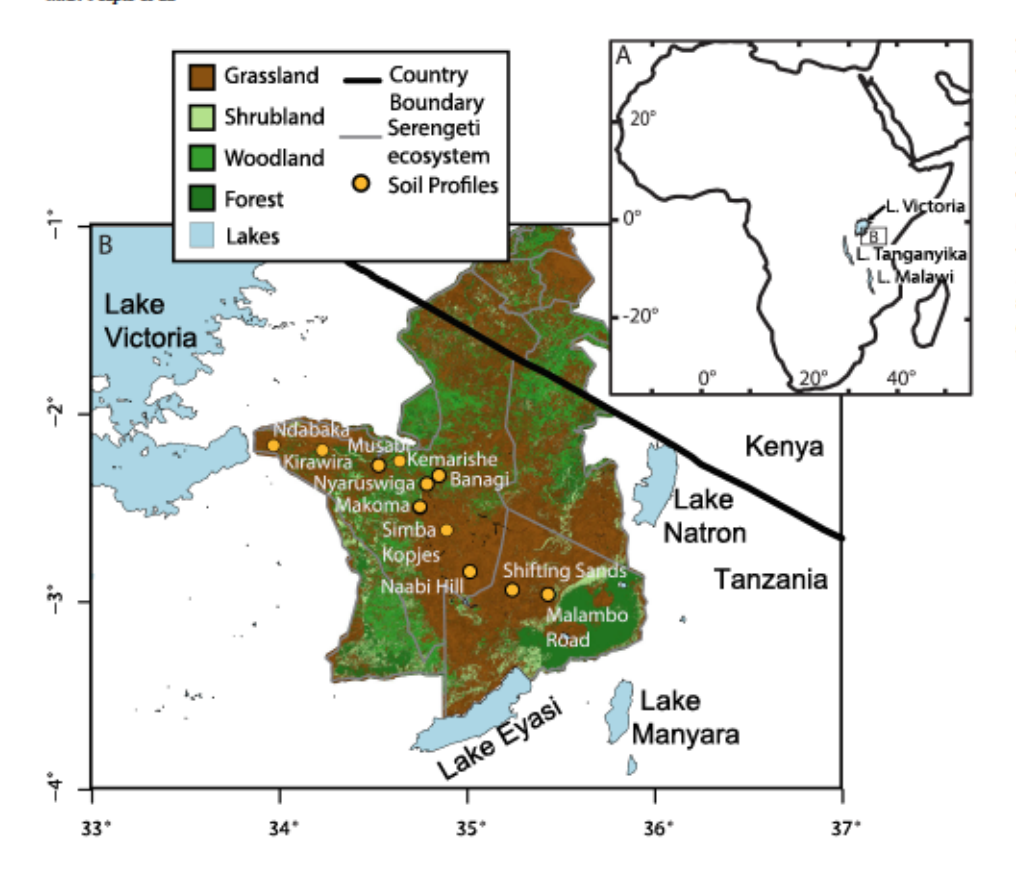


Fig. 1. (A) Location of the Serengeti ecosystem within Africa. (B) Map of study region showing the Serengeti ecosystem spanning Tanzania and Kenya, the soil sampling locations (yellow points) along a transect within the Ngorongoro Conservation Area and Serengeti National Parks in Tanzania. Vegetation map simplified from Reed et al. (2009) to show only grassland, shrubland, woodland, and forest vegetation. Figure from Thang et al. (2021) and reprinted with permission. (For interpretation of the references to colour in this figure legend, the reader is referred to the web version of this article.)

Table 1
Site locations and characteristics.

Site	Latitude	Longitude*	Elevation (masl) <sup>b</sup>	Vegetation <sup>c</sup>	Soil Order	MAAT (°C) °	MTWQ (°C) <sup>6</sup>	MAP (mm/ yr) <sup>e</sup>	PET (mm/ yr) <sup>f</sup>	ΑI	WD (mm/ yr) <sup>f</sup>
Malambo Road	-2.9603	35.4364	1354	Dense grassland	Inceptiool	20.9	22.0	499	1583	0.33	1084
Shifting Sanda	-2.9355	35.2473	1549	Dense shrubbed grassland	Inceptiool	19.8	20.9	558	1521	0.38	963
Naabi Hill	-2.8396	35.0205	1677	Closed shrubbed grassland	Mollisol	19.2	20.1	734	1486	0.52	752
Simba Kopjes	-2.6169	34.8966	1637	Dense to closed grassland	Mollisol	19.6	20.5	805	1521	0.54	716
Makoma	-2.4930	34.7544	1549	Closed treed shrubland	Incepticol	20.2	21.0	829	1560	0.55	731
Nyaruswiga	-2.3496	34.8263	1451	Open treed grazuland to closed grazuland	Mollisol	20.8	21.6	832	1613	0.51	781
Banagi	-2.3290	34.8478	1425	Mixed open grassland to woodland	Inceptiool	20.9	21.8	819	1622	0.51	803
Kemarishe	-2.2498	34.6448	1315	Open grassed woodland	Alfiaol	21.6	22.3	834	1659	0.51	825
Musabi	-2.2719	34.5339	1278	Closed grassland	Mollisol	21.9	22.5	830	1659	0.51	829
Kirawira	-2.1883	34.2322	1215	Dense to closed grassland	Mollisol	22.4	22.9	838	1655	0.53	817
Ndabaka	-2.1654	33.9734	1153	Dense to closed grassland	Vertic Mollisol	22.8	23.2	846	1642	0.55	796

<sup>\*</sup> datum WGS 1984.

b meters above sea level.

e vegetation from Reed et al. (2009).

d Soil Order identified based on field observations and climate, to provide a general understanding of soil type, but is not intended to be an absolute USDA soil

MAAT = Mean Annual Air Temperature, MTWQ = Mean Temperature Warmest Quarter, MAP = Mean Annual Precipitation from Fick and Hijmans (2017).

<sup>&</sup>lt;sup>f</sup> PET = Potential Evapotranspiration using the methods of Hargreaves and Samani (1985), AI = Aridity Index, and WD = Water Deficit from Zomer et al. (2007, 2008). Modified from Beverly et al. (2021).

#### 3.3. GDGT preparation and analyses

Lipid extractions from these soils were previously described (Zhang et al., 2021). Briefly, in that study, soil samples were freeze dried and lipids were extracted from 26 g to 85 g of soil by Accelerated Solvent Extraction at the University of Southern California. The neutral polar fraction, containing GDGTs, was isolated by column chemistry and the purified fractions were stored at 20 °C. For this study, the neutral polar fractions were dissolved in hexane:isopropanol (99:1, v/v) and filtered through a 0.45 m polytetrafluoroethylene filter. Samples were then injected into an Agilent 1260 high-performance liquid chromatograph (HPLC) coupled to an Agilent 6120 mass spectrometer at the University of Arizona. Separation of the GDGTs was accomplished using two Ethylene Bridged Hybrid (BEH) Hydrophilic Interaction (HILIC) silica columns (2.1 mm 150 mm, 1.7 m; Waters) following the method of Hopmans et al. (2016). Single ion monitoring (SIM) of the protonated molecules (M H ions) was used to detect and quantify GDGTs with abundances determined by comparison to a  $C_{46}$  internal standard at m/z744 (Huguet et al., 2006). As the relative response factor between the internal standard and brGDGTs was not monitored, these concentrations should be considered semi-quantitative.

We report concentrations of summed branched ( brGDGT) and isoprenoidal ( isoGDGTs) GDGTs per unit mass of soil (ng/g) and normalized to OC in ng/g OC as summed branched ( brGDGT) and isoprenoidal ( isoGDGTs), as well as the concentrations of individual compounds that are further used in a range of index calculations as follows. In order to assess the temperature information in the brGDGT abundances, we calculated the MBT'<sub>5Me</sub> (De Jonge et al., 2014b; Hopmans et al., 2016) where:

We also calculated the pH sensitive CBT' index (De Jonge et al., 2014b) where.

CBT' has been globally calibrated to pH:

(3

The  $IR_{6Me}$  index expresses the relative amount of C6 vs C5 methylated brGDGTs (De Jonge et al., 2014a) and is thought to be higher in soils with a lower moisture content (Dang et al., 2016) and has shown a significant correlation to soil pH (Naafs et al. 2017).

(4)

We also quantified the isoprenoid GDGTs. In addition to the isoGDGTs, we calculated the Branched and Isoprenoidal Tetraether (BIT) index:

where Ia, IIa and IIIa represent the abundances of both the 5' and 6' methyl isomers of the non-cyclic terrestrial brGDGTs (from soil acid-obacteria) and Cren represents the abundance of crenarchaeol (Hopmans et al., 2004). BIT is commonly used in aquatic depositional settings to detect terrestrial soil inputs assuming soils have a BIT 1; however, in arid soils values 1 have been reported (Dirghangi et al., 2013; Yang et al., 2014). The relative amount of isoGDGTs in soils has been proposed to be an index for aridity (Xie et al., 2012) where:

(6)

The archaeol caldarchaeol ecometric (ACE) was developed as a

proxy for salinity in aquatic settings, and is based on the relative abundance of archaeol (considered to represent halophilic archaea) vs caldarchaeol (also referred to as isoGDGT-0) (Turich and Freeman, 2011):

\_\_\_\_\_(7)

Here we assess the ACE response to soil salinity.

#### 4. Results

## 4.1. Soil temperature and pH measurements

In situ measurements of soil temperatures range from 16.7 C to 30.2 C at depths ranging from 20 cm to 30 cm, as previously reported by Beverly et al. (2021). Soil temperatures are warmer than the interpolated mean annual temperatures which range from 19.2 C to 22.8 C (Fick and Hijmans, 2017; Beverly et al., 2021) and measured MAAT of 21.0 C (Jager, 1982). These soil samples therefore contribute to our understanding of proxy performance and environmental interpretations at the warm end of global soil calibrations (Fig. 2A) and grassland or bare soil settings where soil temperatures can be hotter than air temperatures (Molnar, 2022). In addition, we measured soil pH and find surface soil pH values range from 6.6 to 9.0 with a median value of 8.7 (Fig. 2B; Pangaea dataset; Peaple et al., 2021a). Deeper samples typically have a higher pH than surface samples with a range of 7.4 10.3 and a median value of 9.1. Our data fills a gap in current GDGT compilations which contain few data from high pH soils.

## 4.2. Depth profiles

We report the GDGT compositions at 11 sites, and 26 samples across the Serengeti, including relative and absolute abundances (Pangaea dataset; Peaple et al., 2021a). Within soil profiles at individual sites, brGDGTs (Fig. 3A) and isoGDGTs (Fig. 3B) decrease with depth, mirroring the declines from surface downward in the TOC from 3% at the surface to 0.14% at depth (Fig. 3C) (Zhang et al., 2021). brGDGTs decline from 4 to 168 ng/g at the surface to 2  $\,$  29 ng/g below the surface (Fig. 3A). Normalizing brGDGTs for TOC, we find brGDGTs (Fig. 3D) range from 427 to 9009 ng/g OC at the surface to 348  $\,$  11561 ng/g OC at depth (deepest samples at 1 1.6 m). isoGDGTs decline from surface concentrations of 1 10 ng/g to 1 5 ng/g at depth (Fig. 3B). isoGDGTs range from 79 to 803 ng/g OC at the surface to 87 883 ng/g OC at depth (Fig. 3E, deepest samples at 1 1.6 m). The decline in isoGDGT concentration is proportional to that of TOC such that isoGDGTs are relatively invariant. The ratio between isoGDGTs and brGDGTs (R<sub>i/b</sub>, Fig. 3F) is relatively invariant with depth, with all sites except Malambo Road having an R<sub>i/b</sub> of 0.51 demonstrating the greater abundance of brGDGT molecules relative to isoGDGT. Malambo Road has an R<sub>i/b</sub> of 0.89 at the surface and 1.1 at 0.8 m depth, indicating an almost equal abundance of brGDGT and isoGDGT compounds. BIT is also relatively low at the surface of Malambo Road (0.57), although it increases to 0.91 at 0.8 m depth. Apart from Shifting Sands which has a surface BIT of 0.67, all other sites have BIT values 0.8 (Fig. 3G). Plant wax concentrations measured from paired samples (Zhang et al., 2021) show decreases with depth (Fig. 3O, P) that are proportional to the decreases in TOC%. There is no consistent trend in changes in  $IR_{6Me}$  with depth (Fig. 3K), with some sites showing large 0.2 increases (e.g., Banagi and Nyaruswiga), other sites showing little change ( 0.1) with depth (e.g., Makoma and Kirawira) and other sites showing small decreases (e.g., Musabi).

The temperature-sensitive MBT  $_{5Me}$  proxy is observed to increase with depth in most profiles (Fig. 3I), with surface sample (mean 0.82, standard deviation 0.07) vs deeper samples (mean 0.89, standard deviation 0.07). These values predict BayMBT $_0$  temperatures of

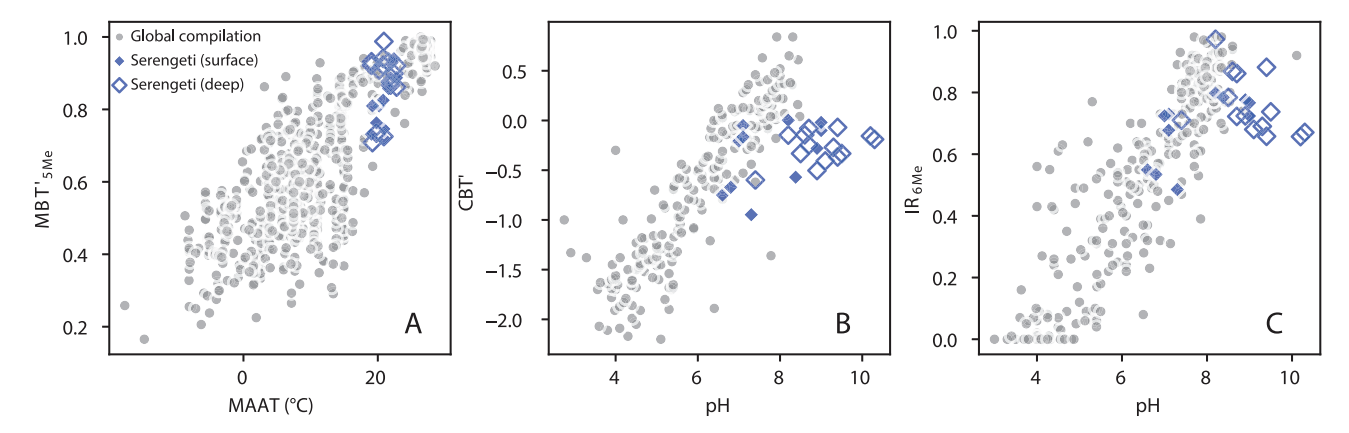


Fig. 2. Serengeti soil data compared to prior global surface soil calibrations. (A) Mean annual air temperature (MAAT) plotted against  $MBT^*_{5Me}$  for the global compilation of surface soil samples (grey symbols) (Dearing Crampton-Flood et al., 2020) and the surface ( 0.1 m; solid blue symbols) and deep ( 0.1 m; open blue symbols) soil samples from this study. (B) Soil pH plotted against CBT' from a global compilation of surface soil samples (De Jonge et al., 2014a) and soils from this study. (C) Soil pH plotted against  $IR_{6Me}$  in both a global compilation (Dearing Crampton-Flood et al., 2020) and soils from this study. (For interpretation of the references to colour in this figure legend, the reader is referred to the web version of this article.)

20.6 C (surface) and 23.2 C (deep), implying a warming trend with depth that is not expected from theory, nor represented by ambient measurements of soil temperature by soil-temperature dataloggers (Beverly et al., 2021). The community index (De Jonge et al., 2019) (not shown) correlates strongly with MBT  $_{\rm 5Me}$  (r 0.99, p 0.0001) and consequently shows similar trends with soil depth (Fig. 3I). Community index values are 0.6 throughout the dataset and are thereby consistently in the warm cluster.

The pH sensitive CBT' shows an increase of 0.25 down profile in Ndabaka, Nyaruswiga and Kirawira with relative invariance with depth in the other sites (Fig. 3J). Measured pH increases with depth at all sites except Musabi where it is invariant (Fig. 3N). The ACE index (salinity proxy) (Fig. 3H) increases with depth at all sites, with surface samples having a mean value of 12 compared to deeper samples which have a mean value of 53. Similarly, TDS (a measure of salinity) (Fig. 3M) values also generally show large increases with depth (deepest samples 1.7 29.5 times greater TDS than surface samples), except for Kirawira which sees a large increase followed by a decrease at the bottom of the profile. For comparison, we also show that TOC <sup>13</sup>C increases with depth in most profiles (Fig. 3L), with Makoma, Banagi and Kemarishe showing especially large 3‰ increases in <sup>13</sup>C with depth (Zhang et al., 2021).

## 4.3. Surface soil GDGT concentrations

Surface soil brGDGT concentrations fall in the range 4 168 ng/g, with a mean of 32 ng/g (Fig. 3A). Concentrations of isoGDGTs are in the range 1 10 ng/g with a mean of 3 ng/g (Fig. 3B). The  $R_{i/b}$  and BIT ranges from 0.01 to 0.89 and from 0.57 to 0.99 respectively (Fig. 3F,G). The BIT index shows a positive correlation with MAP (Fig. 4A) (r 0.87, p 0.01) and the  $R_{i/b}$  shows a negative correlation with MAP (Fig. 4B) (r 0.83, p 0.01). TOC%-normalized isoGDGTs correlate negatively with precipitation (r 0.85, p 0.01) (Fig. 4D) with the two lowest precipitation sites (Shifting Sands and Malambo) having on average 4 times the amount of isoGDGTs compared to the wetter sites, with the correlation driven by lower TOC values at the drier sites. brGDGTs show a weaker non-significant positive correlation with MAP (r 0.29, p 0.38) (Fig. 4C).

## 4.4. Temperature

Based on the relative abundances of the brGDGTs in each soil sample, we calculated MBT' $_{5Me}$  index and then predicted temperatures using BayMBT $_{0}$ , a Bayesian model calibrated to months above freezing (MAF), which is the average temperature of all months 0 C (Dearing

Crampton-Flood et al., 2020), which is the same as MAAT in tropical Africa. BayMBT<sub>0</sub> calculated surface air temperatures fall within the MAAT climatology for the region (Fig. 5A) but are cooler (2 4 C) than the corresponding measured soil temperature (Fig. 5C). Considering the Serengeti soils in isolation, the temperature span of the transect is limited, nevertheless BayMBT<sub>0</sub> temperatures from surface soils (0 0.1 m) show a strong correlation with site MAAT (r 0.73, p 0.01) and a low RMSE (1.8) (Fig. 5A). If added to the global compilation these new surface soil data would bolster observations for the under-sampled warm end of the global calibration (20 25 C). While the global compilation only considers surface soils, brGDGTs at depth are not yet well described. Here we find in deep soil ( 0.1 m) there is no correlation between MAAT and the BayMBT<sub>0</sub>-predicted temperatures (Fig. 5B).

There is a weak correlation between the mean annual precipitation and the temperature regression residuals although the small number of low precipitation sites (n  $\,$  2) precludes further comment on a causal relationship (Fig. 6A). The ratio of 6 vs 5 methyl groups in Serengeti soil samples (IR<sub>6Me</sub>) is relatively high (median  $\,$  0.72) and is correlated with the MAAT absolute residuals (measured-predicted temperature) r 0.69, p  $\,$  0.01 (Fig. 6B).

Across the longitudinal transect, the  $BayMBT_0$ -predicted temperatures from surface soils show a similar pattern to the MAAT, with lower temperatures in the higher elevation eastern part of the transect and higher temperatures in the lower elevation west section (Supplementary Fig. S1). There are no clear trends in the residuals associated with longitude.

# 4.5. pH

The CBT' index yields inferred pH estimates that are lower than measured values, and CBT' values for these alkali soils (up to pH 9) are lower than those measured at pH 6 elsewhere in the world, demonstrating an issue with the application of the global calibration at our sites, and emphasizing the need for studies in alkali soils (Fig. 2B). Surface samples showed a weak non-statistically significant positive relationship between measured pH and predicted pH (r 0.45, p 0.17, Fig. 5E), with an RMSE of 1.4. Measured samples are uniformly more alkaline than CBT' based pH predictions. Samples collected at depth 0.1 m had a weaker, non-significant relationship between measured pH and predicted pH (r 0.39, p 0.17) (Fig. 5F) and plotted outside of the global calibration range (Fig. 2B).

The pH residual is greatest at both the far eastern and western ends of the transect (Supplementary Fig. S1). This residual correlates with TOC in the surface soil (r 0.83, p 0.01), likely a consequence of the

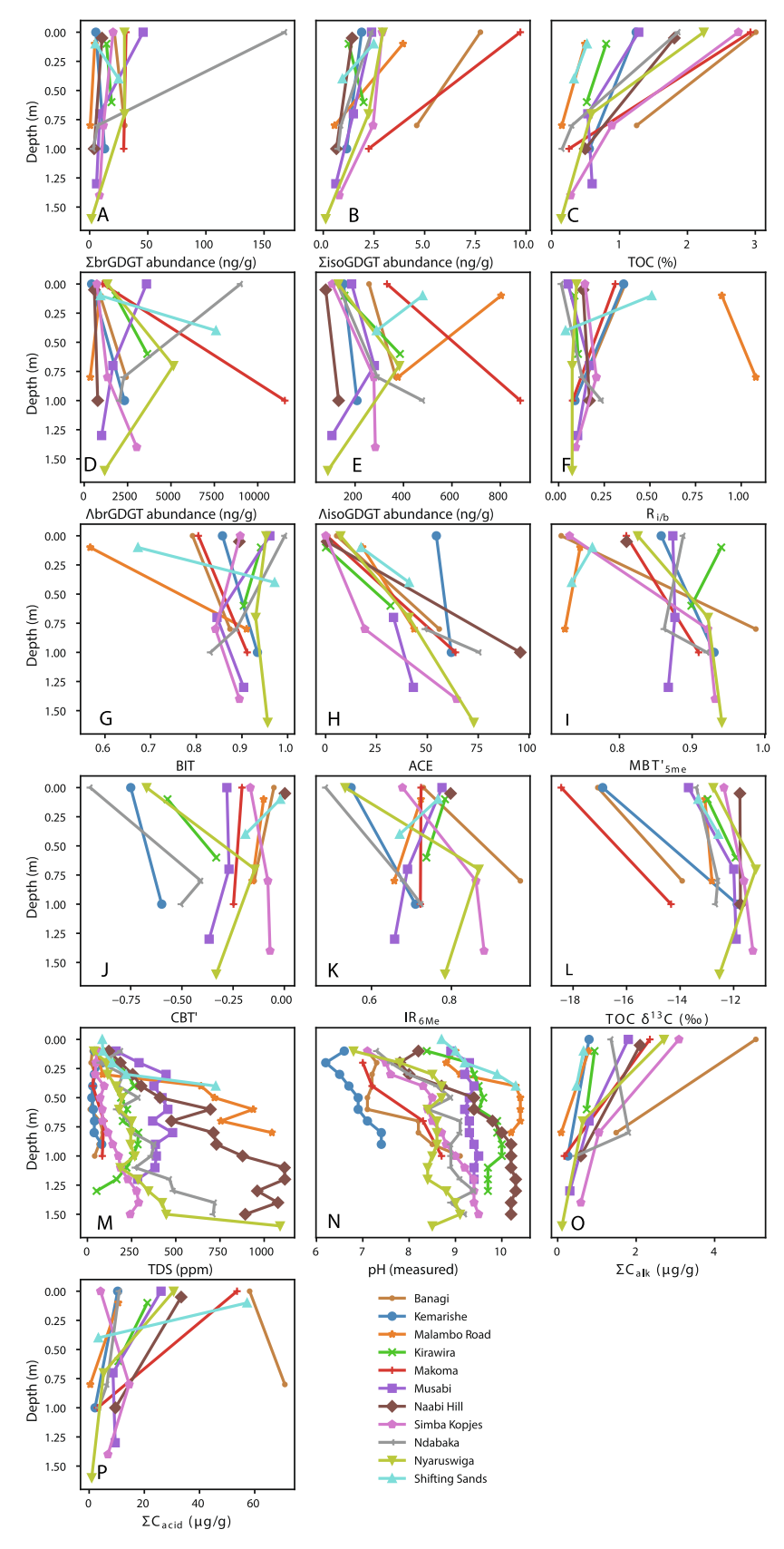


Fig. 3. Depth profiles showing: (A) brGDGT concentrations, (B) isoGDGT concentrations, (C) Total organic carbon (TOC) % (Zhang et al., 2021), (D) brGDGT concentrations, (E) isoGDGT concentrations, (F)  $R_{i/b}$ , (G) BIT, (H) ACE, (I) MBT $_{5Me}$ , (J) CBT $_{5Me}$ , (J) CBT $_{5Me}$ , (L) Total organic carbon  $^{13}$ C (TOC  $^{13}$ C) (Zhang et al., 2021), (M) Total dissolved solids (TDS), (N) Measured pH, (O)  $^{13}$ C  $^{13}$ C

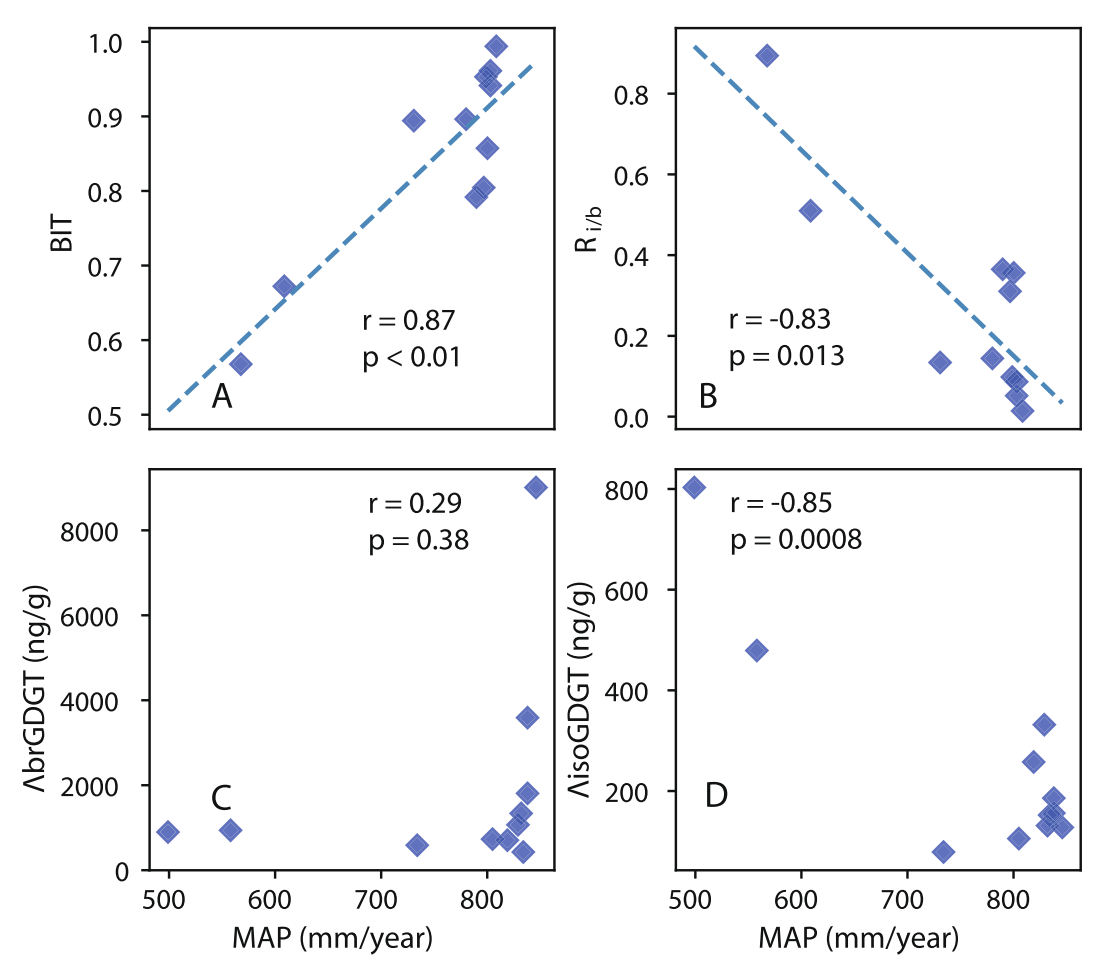


Fig. 4. Relationship between mean annual precipitation (MAP) and surface samples: (A) BIT, (B)  $R_{l/b}$ , (C) brGDGT concentrations (ng/g OC), (D) isoGDGT concentrations (ng/g OC).

strong correlation between TOC% and measured pH (r 0.78, p 0.01). The two driest sites (Shifting Sands and Malambo) both have the highest measured pH in the soil surface (Fig. 3N), although high pH is not exclusive to low precipitation sites the mean pH for MAP 550 mm/year 7.5 whilst the mean pH for sites with MAP 560 mm/year 9.7. A positive correlation (r 0.67, p 0.05) exists between IR<sub>6Me</sub> and pH in surface samples (Fig. 2C) although this is not present in deeper more alkaline samples (r 0.44, p 0.12).

## 5. Discussion

## 5.1. GDGT concentrations

There is a relationship between the relative amounts of  $\;\;$  brGDGT and  $\;\;$  isoGDGT (R $_{i/b}$ ) and the mean annual precipitation at the soil sites (Fig. 4B). The R $_{i/b}$  shows a negative correlation with MAP (r  $\;\;$  0.73, p

0.01 correlation driven by the two driest sites) and the BIT index shows a positive correlation with MAP (r 0.83, p 0.01). As MAP is loosely related to soil moisture content, we interpret that the soil moisture content is controlling  $R_{\rm i/b}$  in the surface soils. The same relationship between MAP and both  $R_{\rm i/b}$  and BIT has been observed in some arid and semi-arid Chinese and North American soil sites (Yang et al., 2014; H. Wang et al., 2017) where it was primarily driven by changes in the brGDGT concentration, with the absolute isoGDGT concentrations less responsive to changing moisture conditions. We observe the same relationship here (Fig. 4C,D), with the two lowest MAP soil sites (Shifting Sands and Malambo Road) having substantially lower mean brGDGT than the wetter sites (5 vs 39 ng/g respectively) (Fig. 3A). In

down-profile samples the relationship of decreased BIT values in arid regions with a MAP  $\,$  600 mm/yr does not persist as values converge to 1 in the lower soil horizons (Fig. 3G). Likewise, the elevated  $R_{i/b}$  values in arid regions also decrease towards 0 in most profiles (Fig. 3F). This pattern can likely be explained by the disproportionate decrease in

isoGDGTs resulting from a decrease in the activity of isoGDGT-producing aerobic archaea of the phylum Thaumarchaeota due to lower oxygen availability. This interpretation is in line with previous studies that have suggested that the low BIT and high  $R_{i/b}$  values in arid areas result from the favorable conditions for NH $_3$  oxidation by Thaumarchaeota in these environments (Xie et al., 2012; Dirghangi et al., 2013).

As in most soil profiles, TOC declines with depth and so do the biomarker concentrations (Fig. 3A E, O, P) linked to the processes of surface inputs and downward mixing and decay. We find the concentration of isoGDGTs in the soil profiles is strongly correlated with the TOC% of the sample (r 0.75, p 0.01) although brGDGTs show a much weaker and non-significant correlation (r 0.35, p suggesting that brGDGT production or preservation is only partly related to that of isoGDGTs and TOC. The magnitude of the decline with depth differs with GDGTs declining proportionally less than TOC (median 62% decline of isoGDGTs, 58% of brGDGTs vs 70% for TOC), suggesting that these molecules are relatively resistant to degradation compared to other components of organic matter, as also reported in previous studies on soils (Huguet et al., 2010) as well as in loess-paleosol sequences (H. Wang et al., 2017). An increase in the amount of brGDGTs with depth was recorded in 7 out of 15 samples, which we interpret as representing in situ production of brGDGTs in addition to a fossil brGDGT component.

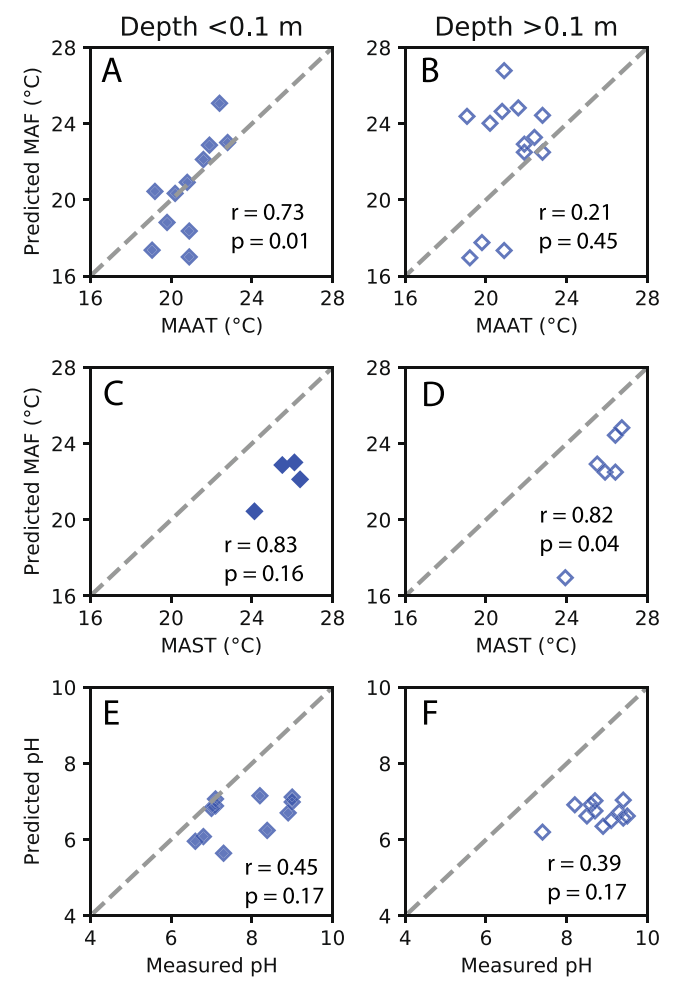


**Fig. 5.** Comparison of measured mean annual soil temperature (MAST) and predicted soil temperature, modeled air temperature and pH at both the surface (left column, filled blue symbols) and at depth (right column, open blue symbols). (A) and (B): Cross plots of mean annual air temperature (Fick and Hijmans, 2017) against mean temperature from months above freezing (MAF) predicted by BayMBT<sub>0</sub>. (C) and (D): Cross plots of measured soil temperature at nearest depth to brGDGT sample (Beverly et al., 2021) against BayMBT<sub>0</sub>. (E) and (F): Cross plots of measured soil pH against CBT predicted pH. (For interpretation of the references to colour in this figure legend, the reader is referred to the web version of this article.)

Whilst downward mixing could in theory result in the transfer of more organic rich surface soil deeper into a soil profile, we see declines in the TOC% with depth at every soil site indicting that this explanation is

unlikely.

#### 5.2. ACE and soil salinity

In these dryland soils, with salts and carbonate precipitating, we find an increase in total dissolved solids with depth (Fig. 3M) as well as variations between sites, with the more alkaline sites (e.g., Shifting Sands) showing higher salt concentrations. TDS variations between sites and with depths covary with organic concentrations (Fig. 7) with deeper, more saline sites samples having less TOC. We find an inverse power law relationship between total dissolved solids, a proxy for salinity, and bulk organics (Fig. 7C) and the concentration of isoGDGTs (Fig. 7A) but not with brGDGTs (Fig. 7B). Soil salinity can affect soil organic carbon content in two ways: (1) by decreasing the input of plant and microbially derived carbon into the soil or (2) by reducing the rate of decomposition and thus increasing organic carbon (Setia et al., 2013). However, TDS also increases with depth (Fig. 3H) so this relationship could be explained by deeper samples having undergone more organic degradation (Fig. 7D F). However, we find a stronger relationship between TDS and isoGDGTs (Fig. 7A) than depth and isoGDGTs (Fig. 7D) (r<sup>2</sup> 0.64 vs 0.34) suggesting that TDS content is the controlling variable. Additionally, we calculated a partial correlation coefficient of r 0.67, p 0.01 between TDS and isoGDGTs whilst controlling for depth, showing that TDS and isoGDGTs are correlated even when accounting for depth. Whilst TOC has a stronger relationship with depth than TDS ( $r^2$  0.66 vs 0.52) when considering all the samples, if the surface samples are excluded there is no relationship between depth and TOC, yet there is between TDS and TOC (r<sup>2</sup> 0.01 vs 0.35) suggesting that again TDS is the controlling variable. We also calculated a partial correlation coefficient of r 0.40, p between TOC and TDS whilst controlling for depth. As such, it appears that increased salinity leads to increased organic carbon degradation and a power law relationship explains both the inverse relationship with

but to a lesser extent that of the brGDGTs. We also see a change in the ACE index with depth (proportion of halophilic-biomarker archaeol vs halophobic-biomarker caldarchaeol), with surface samples having notably lower ACE values than deeper samples (mean surface 12. 1 18, mean deep Fig. 3H). The ACE index has traditionally been applied to marine (Turich and Freeman, 2011) and lacustrine water samples (Wang et al., 2013; He et al., 2020; Peaple et al., 2021b) to track the relative proportion of halophilic archaea and Euryarchaeota which produce both archaeol and GDGT-0, caldarchaeol . As halophilic archaea are known to inhabit saline soils (e.g., Lizama et al., 2001), we assessed ACE in what we believe is the first such application to soils. Over all samples and sites, we see a moderate positive correlation of r 0.55, p 0.01 between ACE and total dissolved solids in our samples (Fig. 8), which suggests that the proportion of halophilic archaea in soils and thus the ACE index

depth as well as the variations between sites for TOC and isoGDGTs

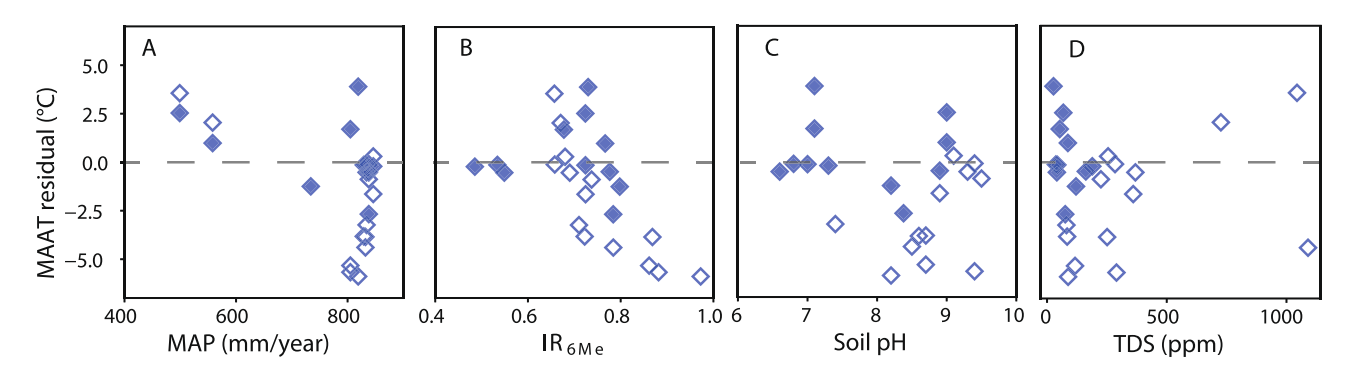


**Fig. 6.** Exploring possible factors influencing mean annual air temperature (MAAT) residuals (MAAT-predicted MAAT) in all soil samples (surface 0.1 m, solid symbols; deep 0.1 m, open symbols), including (A) mean annual precipitation (MAP), (B) IR<sub>6Me</sub>, (C) measured pH and (D) total dissolved solids (TDS). Gray dashed line represents 0 residual.

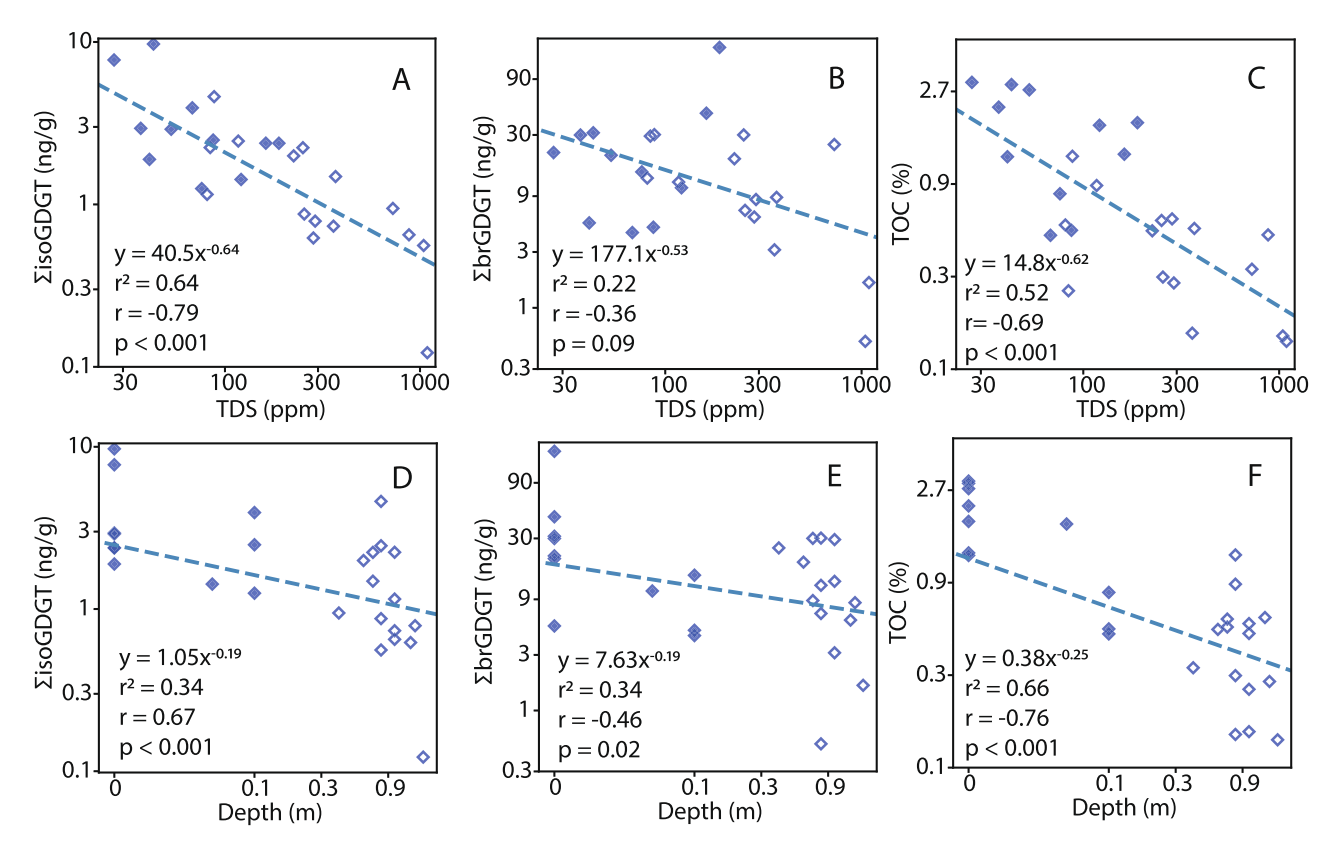
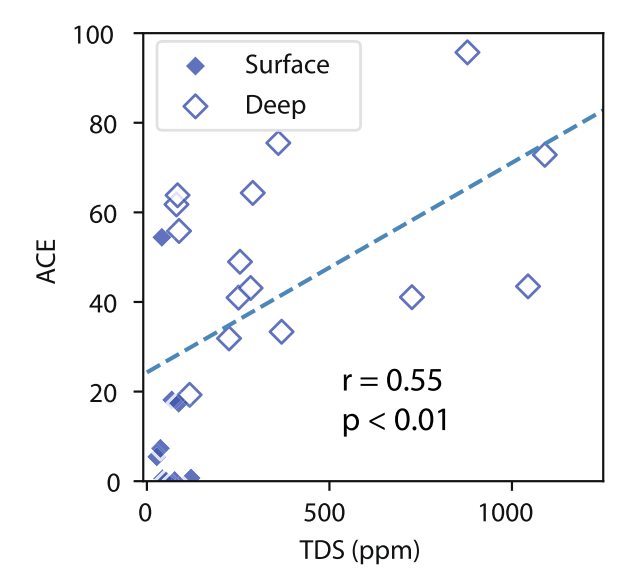


Fig. 7. Comparison of total dissolved solids (TDS) vs (A) isoGDGTs, (B) brGDGTs and (C) TOC and sampling depth vs (E) isoGDGTs, (F) brGDGTs and (G) TOC. We show the amount of variance explained by a power law regression as well as the Spearman rank correlation coefficient and corresponding p value. Solid blue symbols represent surface samples and white filled symbols represent deep soil samples. (For interpretation of the references to colour in this figure legend, the reader is referred to the web version of this article.)



**Fig. 8.** Cross plot of measured total dissolved solids (TDS) and calculated ACE index in soil samples, showing surface samples (solid symbols) and deep (open symbols).

responds linearly to salinity, similar to the behavior of archaea and ACE in hypersaline, aquatic settings.

## 5.3. Factors influencing BayBMT<sub>0</sub> in Serengeti soils

Low mean annual precipitation (MAP) has been reported to lead to

higher MAAT residuals (Peterse et al., 2012; De Jonge et al., 2014b; Menges et al., 2014; Dang et al., 2016). The recent global soil compilation (Dearing Crampton-Flood et al., 2020) reported no correlation between MAP and MAAT residuals; however, there was a greater variance in samples from MAP 500 mm/year. In this study, we see that both surface and deep soil samples from lower precipitation sites have positive temperature residuals (1.8 C vs 2.8 C respectively, Fig. 6A) and the mean absolute residual is slightly higher than from the higher precipitation samples although the low sample size for the 560 mm/yr (n 4) precludes firm conclusions.

Additionally, the proportion of 5 to 6 methylated compounds (IR $_{6Me}$ ) may affect the MBT' $_{5Me}$  temperature proxy skill, with samples with a greater proportion of 6 methylated compounds (IR 0.5) having brGDGT distributions that were less responsive to temperature (Dang et al., 2016; Naafs et al., 2017). However, recent global compilations show that the effect is limited to IR 0.8 (Dearing Crampton-Flood et al., 2020). Here we also find evidence for a threshold at IR $_{6Me}$  0.8 among the deep samples, with samples with an IR $_{6Me}$  0.8 having a large negative MAAT residual (Fig. 6B) implying the BayMBT $_0$  predicted temperatures have a warm bias (mean 5.2, n 4) vs small residuals in those with IR 0.8 (mean 1.7, n 21).

pH can have a significant although not unidirectional effect upon MBT'<sub>SMe</sub> values (De Jonge et al., 2019, 2021; Halffman et al., 2022) due to the influence of changing bacterial community composition on brGDGT lipid relative abundance. Among the surface samples in our study, pH does not have a relationship with MAT residuals, but there are trends in the MAT residuals with regards to the deeper samples with less alkaline samples having more negative residuals, implying a bias toward warmer predicted temperatures (Fig. 6C). We tested the hypothesis that the mean temperature residuals were different between deep high pH samples (pH 9) and deep lower pH (pH 9) by performing a one-way

ANOVA test. We found that the mean residual for the deep low pH samples was greater than the high pH samples (4.0 vs 1.9 respectively) and that this difference was statistically meaningful (F value (5.2) F critical value (4.7) and p 0.05).

Salinity has been demonstrated to impact MBT $^{\prime}_{5Me}$  values in lakes (Wang et al., 2021), by controlling the isomerization of brGDGTs. Although some previous soil-based brGDGT studies found a negative correlation between MBT $^{\prime}_{5Me}$  and soil salinity (Zang et al., 2018), other studies did not (Dang et al., 2016). In this study, we do not find salinity affects the MAAT residuals (Fig. 6D), suggesting it is not playing a significant role in determining brGDGT distributions in these Serengeti soils.

## 5.4. Offsets between surface and deep brGDGT predicted temperatures

Whilst brGDGTs samples from surface soils are reflective of modern MAAT, and to a lesser extent pH (Fig. 5A,C,E), there is no relationship between deeper samples and modern surface environmental conditions (Fig. 5B, D, F). Previous studies have also reported significant variability in soil MBT (Davtian et al., 2016) and MBT 5Me with depth (Pei et al., 2021) with potential explanations focused on modern production under lower oxygen conditions in deeper soils (Pei et al., 2021), land use changes, degradation and varying chemical compositions down profile (Daytian et al., 2016). In a collection of Vietnamese soils (Daytian et al., 2016), Podzols were identified as showing large decreases in MBT' with depth relative to the surface soils, although other soil types did not show this change. Changes in CBT (pH sensitive cyclization of branched tetraethers index) with depth were variable and did not depend on soil type (Davtian et al., 2016). Lower oxygen conditions were linked to higher MBT' and lower CBT in soils sampled from Zhoukoudian and Mt. Changbai, China through a modulation of the bacterial community (Pei et al., 2021).

The distributions of core brGDGTs (measured in this study) are thought to be resistant to degradation (Schouten et al., 2004) and stable over geological time scales (e.g., M. Wang et al., 2017; Lu et al., 2019). As such, whilst the overall concentration of GDGTs in our study decreased with depth (Fig. 3A,B) there is no reason to assume that this will impart a bias on the MBT'5Me index, given the structural similarity of the brGDGT molecules involved in its calculation. As such, degradation is unlikely to be a large factor in down profile changes in MBT'5Me. In

addition, given that the soil temperature loggers show that there is no change in the mean soil temperature with depth (Beverly et al., 2021) it is unlikely that temperature differences between surface and deep soils would cause the offset in MBT' $_{\rm 5Me}$ . Whilst low oxygen levels have previously been implicated in high MBT' $_{\rm 5Me}$  bias in deep soils (Pei et al., 2021) we can also rule out the presence of anoxic conditions in our Serengeti soils due to the lack of gleyed colors and there being no evidence of Fe reduction.

We examined a suite of environmental and biomarker information to attempt to determine if in situ production at depth could explain the predicted temperature offset from the surface. We find that in principal component space, MAP and TOC are positively correlated with MBT'5Me among deep soil samples (Fig. 9B). Whilst MAP is not correlated with MAT residuals in the global BayMBT model, previous studies have shown that MAP 600 mm/year can lead to a cold bias (De Jonge et al., 2014b) in temperature reconstructions. Two dry sites with low TOC (Malambo Road and Shifting Sands) have deep samples with relatively low MBT'5Me (0.73), which could be explained by the low MAP. However, most samples show an increase in MBT'5Me with depth (Fig. 9B). We note that MBT'<sub>5Me</sub> in the deep samples also has a negative correlation with total dissolved solids and pH in principal component space. This corresponds to more saline and alkali soils having lower MBT 5Me values and more acidic, less saline soils having higher MBT'5Me. Changes in pH have been demonstrated to influence the MBT'5Me of surface soils in the absence of a change in temperature, through altering the brGDGTproducing bacterial community (De Jonge et al., 2019, 2021; Halffman et al., 2022). Additionally, out of the three soil profiles studied by Pei et al. (2021) the largest increase in MBT'<sub>5Me</sub> occurred in the highest pH soil (pH 8). As the soils in this study are all alkaline this possibly suggests that deep soil high pH conditions biases MBT'5Me higher relative to the surface soil. Given that we find MBT'5Me is responsive to changes in pH only in deep samples, compared to surface samples which respond primarily to MAAT (Fig. 9A), this could suggest that we see modern production of brGDGTs throughout our soil profiles, with different bacterial communities at different depths responsive to different environmental stimuli.

We do not see a large change in the CBT' with depth, with both shallow and deep samples having statistically insignificant correlations between CBT' and soil pH and CBT'-based pH models (De Jonge et al., 2014b) underestimating soil pH. A systematic underestimation of pH

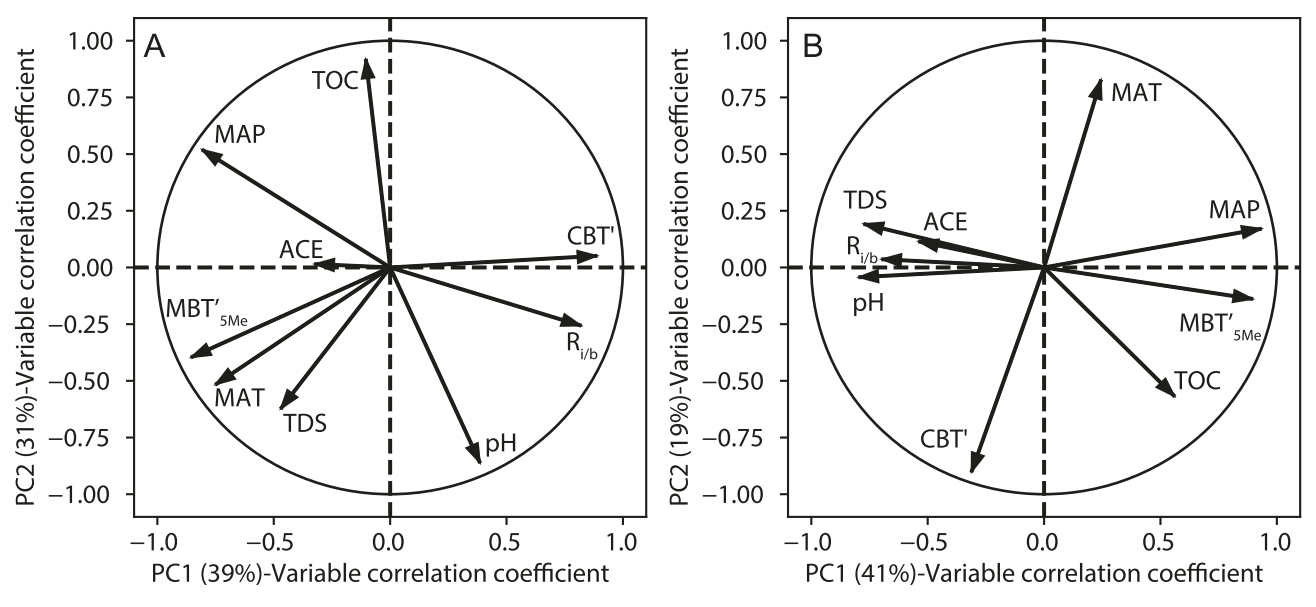


Fig. 9. PCA biplots showing biomarker and environmental indices: Total organic carbon % (TOC), CBT', ratio of isoGDGTs to brGDGTs ( $R_{i/b}$ ), measured pH, total dissolved solids (TDS), mean annual air temperature (MAT; Fick and Hijmans, 2017), MBT'<sub>5Me</sub>, archaeol caldarchaeol ecometric (ACE), mean annual precipitation (MAP; Fick and Hijmans, 2017) for (A) all surface samples ( 0.1 m), (B) all deep samples ( 0.1 m).

using a CBT' soil calibration (De Jonge et al., 2014b) compared to a global compilation (Fig. 2B) suggests that the relative abundance of 6-methyl and/or cyclic brGDGT compounds is controlled in part by something other than pH in our samples. We note that a similar pH underestimation occurs in a suite of dry, alkaline soils sampled from Inner Mongolia (Guo et al., 2022), although CBT' does correlate with soil pH in these samples. There is a moderate correlation (r = 0.67, p < 0.05) between IR<sub>6Me</sub> and pH in our surface soil samples and these values are broadly consistent with a global compilation (Dearing Crampton-Flood et al., 2020) (Fig. 2C) which suggests that the isomerization is responsive to pH. However, the lack of a significant correlation between IR<sub>6Me</sub> and pH in the deeper samples could be caused by the relative proportion of 6-methyl brGDGTs being controlled by other factors possibly including changing bacterial community composition.

#### 5.5. Comparison of organic and carbonate paleothermometers

#### 5.5.1. Proxy comparison in the entire Serengeti dataset

The paired sampling for organics and carbonates within the same soil profiles facilitates a comparison of brGDGT thermometry with carbonate clumped isotope thermometry (Beverly et al., 2021). Across both proxies we find all temperature estimates fall within the range of modern Serengeti soil temperatures of 17-30 °C and the median temperature (across all samples) generated from each proxy is identical (23 °C, Fig. 10A). Despite proxy analytical uncertainty, possible differences in time integration of each proxy and inter-sample variability (aspects that will be discussed further in Section 5.5.4), both proxies on average generate temperatures that are comparable and correlate with MAAT (Fig. 10B). We note that the Serengeti experiences small seasonal air temperature changes (Fick and Hijmans, 2017) on account of its equatorial position, which likely precludes any complications from proxy formation seasonal biases. Further, the general stability of regional air temperatures over the past few thousand years (Tierney et al., 2008; Berke et al., 2012) would not suggest a bias if the time-span of each recorder differs

#### 5.5.2. Inter- and intra-site proxy comparison

Within the Serengeti transect there is approximately 4 °C spatial variation in MAAT and both proxies capture the temperature gradient across the region (Fig. 10B). The brGDGT-temperatures from deeper soils present a complication in these saline soils, and we find evidence for in situ production. Within depth profiles we find no significant correlation (r=0.16, p=0.60) between predicted brGDGTs and MAAT or carbonate-formation temperatures – intentionally sampled from the same position in the soil for this comparison (Beverly et al., 2021). We also found no correlation (r=0.29, p=0.45) between surface brGDGT samples (in the more organic-rich horizons) with the clumped isotope temperatures derived from soil carbonates (that are found at depth in the profile) – which would reflect how each proxy would be typically sampled in a soil based on organic and carbonate substrate distribution. Even though both proxies show a positive correlation with MAAT (clumped: r=0.60, p=0.09: brGDGT: r=0.73, p=0.01), they do not correlate with each other. This lack of correlation is perhaps unsurprising given the size of the uncertainties (instrumental and calibration), the small temperature range within the Serengeti, and the different processes of formation for each proxy recorder, which we discuss next.

## 5.5.3. Process-based differences between proxy recorders

Both proxies are known to capture different temperature signals, with the brGDGT MBT' $_{5\text{Me}}$  showing a strong positive relationship with months above freezing mean annual air temperature (Dearing Crampton-Flood et al., 2020), with salinity at depth creating a confounding signal in these soils.  $\Delta_{47}$  records the temperature of carbonate precipitation which often reflects warm season temperatures, and which can be modulated by soil grain size, vegetation cover, precipitation seasonality and depth in soil (Kelson et al., 2020). Of these factors, equatorial climates allow us to eliminate concerns over seasonal differences between proxy recorders in this setting. Whilst BayMBT0 temperatures are similar to MAAT,  $\Delta_{47}$  temperatures are typically warmer (Fig. 10B) which is in agreement with previous  $\Delta_{47}$  (Kelson et al., 2020) and MBT' $_{5\text{Me}}$  temperature compilations (Dearing Crampton-Flood et al., 2020).

A clear difference between the two analytes is the difference in their distribution in the profiles: the carbonates are located from 0.4 to 1.6 m and below, whereas the brGDGTs decline in concentrations with depth from 0 to 1.6 m (Fig. 3A). We find that the surface soil brGDGT-based, BayMBT<sub>0</sub>-calibrated MAF temperatures range from 17 °C to 25 °C with a mean of 21 °C (SEM = 0.8 °C, n = 11), whereas samples at depth > 0.1 m range from 17.0 °C to 26.8 °C with a mean of 22.8 °C. Clumped isotopes yield a mean of 23.3 °C (SEM = 5.5 °C, n = 27) that is indistinguishable from the organic proxy within error, but the samples have a larger temperature range (14–31 °C; Beverly et al., 2021).

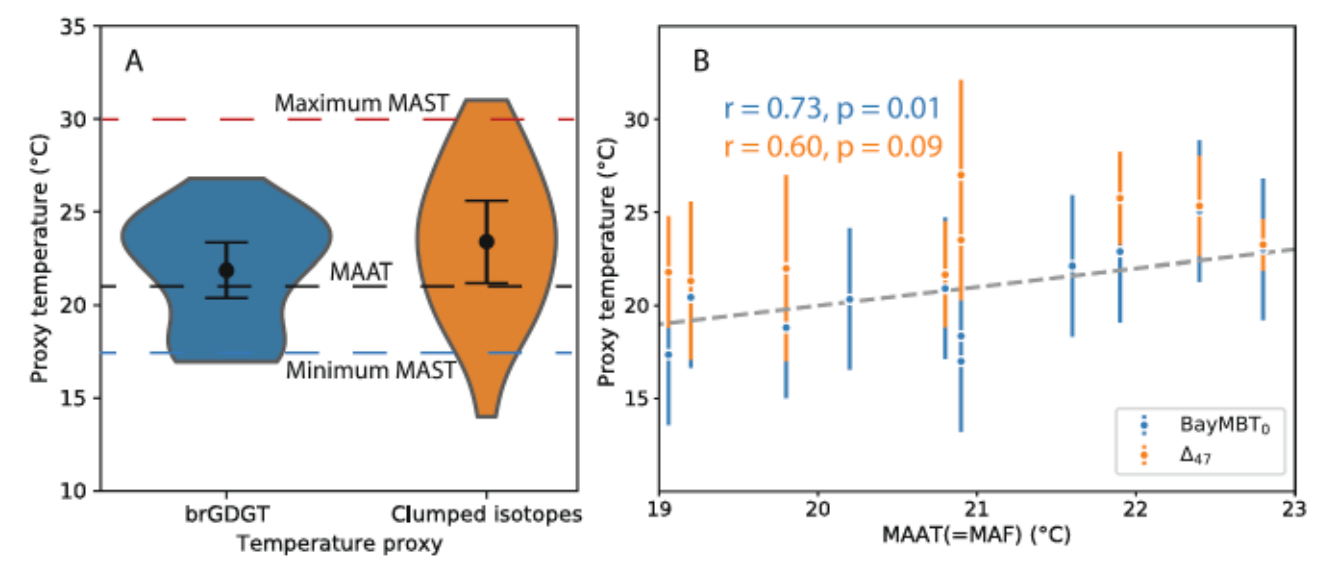


Fig. 10. Comparison of brGDGT (this study) and clumped (Beverly et al., 2021) temperature estimates. (A) Violin plot showing distributions of all samples: central estimates are the same within uncertainties however the range differs. MAAT and minimum and maximum MAST temperatures for the Serengeti shown for comparison. (B) Cross-plot of site MAAT (equivalent to MAF) from surface soil BayMBT<sub>0</sub> (error bars, calibration 1 RMSE) and  $\Delta_{47}$  temperatures within the soil profile (error bars, propagated analytical and calibration uncertainty, 1 SEM); 1:1 line (dashed line).

The analytical and calibration uncertainties of each proxy differ. BrGDGTs have a trivial analytical uncertainty (ca. 0.2 C, Fleming and Tierney, 2016), and are thus measured singly and the uncertainty is dominated by the calibration uncertainty for BayMBT $_0$  to MAF, reported as an RMSE of 3.8 C (Dearing Crampton-Flood et al., 2020).  $_{47}$  records the assumed-thermodynamic formation temperature of carbonate and has been calibrated in laboratory settings (e.g., Ghosh et al., 2006; Bonifacie et al., 2017; Petersen et al., 2019) and in a range of environments. For clumped isotope measurements, the combined instrumental and analytical uncertainties on samples and standard replicates indicate a 1 SEM typically on the order of  $\sim$  4 C (5.5 C in these particular samples; Beverly et al., 2021).

Soils are notoriously spatially heterogeneous, and we find that both pedogenic carbonate nodules and biomarkers in this study show a large variance within soil profiles and across the Serengeti transect which is notable given the relatively small variance in regional spatial and seasonal temperature (Fig. 10A). Meso- and macrofauna homogenize soil microbial communities over multiple meters (Vos et al., 2013), thus this may also be the scale over which molecular biomarkers may be mobile. Similarly soil carbonates form with waters and pore space atmospheres that likely mix over the scale of meters (Zamanian et al., 2016), but localized nodule conditions may differ on a finer scale. While soil carbonate nodules are actively growing in deeper horizons (Beverly et al., 2021), in stable soils such as these they have likely formed over  $10^2$  to 10<sup>3</sup> years (Gallagher and Sheldon, 2016). Soil brGDGT ages are only recently receiving attention, but they are likely modern in surface horizons, and initial compound specific radiocarbon studies in Switzerland indicates they may reach mean ages of 10<sup>3</sup> years at depth (Gies et al., 2021). Microbial production is most active in the high TOC upper soils, with both older fossil biomarkers and living microbial communities present deeper in the profile.

Thus, while the spatial and temporal scales of mixing may be similar, differences in the processes of formation of each proxy, soil heterogeneity and proxy uncertainty likely limit the correspondence that can be achieved at fine scales. We encourage large sample sizes across multiple depths and locations as in this study n 5 was found to significantly reduce the standard deviation of the distribution of means from bootstrapped data (Supplementary Fig. S2). Such an approach is necessary to capture mean conditions with both proxies and helps to average out the observed heterogeneity caused by the inherent spatial heterogeneity of soils as well as the process of formation differences and analytical uncertainty in each. In modern soils the full profile can be studied, but in paleosols the surface soil horizon is sometimes missing in the stratigraphic record (Kraus, 1999) and thus the ability to fully characterize a paleosol profile and thus account for depth-dependent signals identified here (e.g., warm, saline bias at depth) may be curtailed. This emphasizes the importance of soil profile studies to fully characterize and study the processes affecting the spatial signatures of GDGT proxies in depth distributions as relevant to paleosol applications.

## 6. Conclusions

We analyzed the GDGT composition of a suite of soil samples collected across the Serengeti National Park, Tanzania. Surface soil BayMBT<sub>0</sub>-predicted temperatures correlated with MAAT (equivalent to MAF in the tropics). We found deep soil brGDGTs were more responsive to high soil pH and salinity than to mean annual temperature and represent in situ production. We also compared the organic temperature proxy to previously published clumped isotope thermometry on soil carbonates in the same soils. We find that both proxies predict temperatures in the range of modern recorded temperatures, and with large sample sizes their mean values agree. Both proxies detect the temperature gradient across the transect in surface soils, but clumped temperatures are warm-biased as expected in grasslands where soils are often warmer than air temperatures, and deep soil samples have warm-biases for the brGDGT proxy. Further comparison between the two proxies

would be aided by studies in cool climate, carbonate-bearing soils to compare the recorders across a broader range of temperatures and pedogenic settings. These Serengeti soil comparisons show broad proxy agreement, however care should be taken when interpreting brGDGT-derived temperatures below the soil surface, as well as low numbers of 47 samples. Based on our findings here, we encourage more dual proxy paleothermometry and emphasize the need for a large number of analyses (n 5) across multiple soil locations to achieve robust comparison and to explore confounding factors. Notwithstanding the need for further calibration, the potential of dual proxy applications lies in their joint application to a range of modern and ancient soils.

## **Declaration of Competing Interest**

The authors declare that they have no known competing financial interests or personal relationships that could have appeared to influence the work reported in this paper.

## Acknowledgements

This work was supported in part by the National Science Foundation EAR Postdoctoral Fellowship (EAR-PF-1725621) to EB. Samples were collected under permits issued to EB by the Tanzanian government under COSTECH Permit #2018-39-NA-2018-17, TANAPA Research Permit #: TNP/HQ/C.10/13, and TAWIRI Permit #: TWRI/RS-342/2016/116. Thanks to Joseph Masoy and Honest Ndoro for field assistance; Yannick Matia, Efrain Vidal, Daolai Zhang, Nick Rollins and Patrick Murphy for laboratory assistance. We thank the Co-Editor in Chief John Volkman, Associate Editor Stefan Schouten, and reviewers, including Nina Davtian, for their attentive comments that strengthened the manuscript.

## Data availability statement

All data reported here will be made publicly available upon acceptance at Pangaea.

Research Data associated with this article can be accessed at https://doi.org/10.1594/PANGAEA.940031.

## Appendix A. Supplementary material

Supplementary data to this article can be found online at https://doi.org/10.1016/j.orggeochem.2022.104433.

## References

- Anderson, V.J., Shanahan, T.M., Saylor, J.E., Horton, B.K., Mora, A.R., 2014. Sources of local and regional variability in the MBT /CBT paleotemperature proxy: Insights from a modern elevation transect across the Eastern Cordillera of Colombia. Organic Geochemistry 69, 42–51.
- Bai, Y., Chen, C., Xu, Q., Fang, X., 2018. Paleoaltimetry potentiality of branched GDGTs from Southern Tibet. Geochemistry, Geophysics, Geosystems 19, 551 564.
- Berke, M.A., Johnson, T.C., Werne, J.P., Grice, K., Schouten, S., Sinninghe Damste, J.S., 2012. Molecular records of climate variability and vegetation response since the Late Pleistocene in the Lake Victoria basin, East Africa. Quaternary Science Reviews 55, 59–74.
- Beverly, E.J., Lukens, W.E., Stinchcomb, G.E., 2018. Paleopedology as a tool for reconstructing paleoenvironments and paleoecology. In: Croft, D., Su, D., Simpson, S. (Eds.), Methods in Paleoecology. Vertebrate Paleobiology and Paleoanthropology, Springer, Cham, pp. 151–183.
- Beverly, E.J., Levin, N.E., Passey, B.H., Aron, P.G., Yarian, D.A., Page, M., Pelletier, E.M., 2021. Triple oxygen and clumped isotopes in modern soil carbonate along an aridity gradient in the Serengeti, Tanzania. Earth and Planetary Science Letters 567, 116952. https://doi.org/10.1016/j.epsl.2021.116952.
- Bonifacie, M., Calmels, D., Eiler, J.M., Horita, J., Chaduteau, C., Vasconcelos, C., Agrinier, P., Katz, A., Passey, B.H., Ferry, J.M., Bourrand, J.J., 2017. Calibration of the dolomite clumped isotope thermometer from 25 to 350 °C, and implications for a universal calibration for all (Ca, Mg, Fe)CO<sub>3</sub> carbonates. Geochimica et Cosmochimica Acta 200. 255 279.
- Cleveland, D.M., Atchley, S.C., Nordt, L.C., 2007. Continental sequence stratigraphy of the Upper Triassic (Norian Rhaetian) Chinle strata, northern New Mexico, U.S.A.:

- Allocyclic and autocyclic origins of paleosol-bearing alluvial successions. Journal of Sedimentary Research 77, 909–924.
- Coffinet, S., Huguet, A., Pedentchouk, N., Bergonzini, L., Omuombo, C., Williamson, D., Anquetil, C., Jones, M., Majule, A., Wagner, T., Derenne, S., 2017. Evaluation of branched GDGTs and leaf wax *n*-alkane <sup>2</sup>H as (paleo) environmental proxies in East Africa. Geochimica et Cosmochimica Acta 198, 182 193.
- Dang, X., Yang, H., Naafs, B.D.A., Pancost, R.D., Xie, S., 2016. Evidence of moisture control on the methylation of branched glycerol dialkyl glycerol tetraethers in semiarid and arid soils. Geochimica et Cosmochimica Acta 189, 24 36.
- Davtian, N., Menot, G., Bard, E., Poulenard, J., Podwojewski, P., 2016. Consideration of soil types for the calibration of molecular proxies for soil pH and temperature using global soil datasets and Vietnamese soil profiles. Organic Geochemistry 101, 140, 153
- De Jonge, C., Stadnitskaia, A., Hopmans, E.C., Cherkashov, G., Fedotov, A., Sinninghe Damste, J.S., 2014a. In situ produced branched glycerol dialkyl glycerol tetraethers in suspended particulate matter from the Yenisei River, Eastern Siberia. Geochimica et Cosmochimica Acta 125, 476–491.
- De Jonge, C., Hopmans, E.C., Zell, C.I., Kim, J.-H., Schouten, S., Sinninghe Damste, J.S., 2014b. Occurrence and abundance of 6-methyl branched glycerol dialkyl glycerol tetraethers in soils: Implications for palaeoclimate reconstruction. Geochimica et Cosmochimica Acta 141, 97 112.
- De Jonge, C., Radujkovic, D., Sigurdsson, B.D., Weedon, J.T., Janssens, I., Peterse, F., 2019. Lipid biomarker temperature proxy responds to abrupt shift in the bacterial community composition in geothermally heated soils. Organic Geochemistry 137, 103897. https://doi.org/10.1016/j.orggeochem.2019.07.006.
- De Jonge, C., Kuramae, E.E., Radujkovic, D., Weedon, J.T., Janssens, I.A., Peterse, F., 2021. The influence of soil chemistry on branched tetraether lipids in mid- and high latitude soils: Implications for brGDGT- based paleothermometry. Geochimica et Cosmochimica Acta 310, 95–112.
- Dearing Crampton-Flood, E., Tierney, J.E., Peterse, F., Kirkels, F.M.S.A., Sinninghe Damste, J.S., 2020. BayMBT: A Bayesian calibration model for branched glycerol dialkyl glycerol tetraethers in soils and peats. Geochimica et Cosmochimica Acta 268, 142 159.
- Dirghangi, S.S., Pagani, M., Hren, M.T., Tipple, B.J., 2013. Distribution of glycerol dialkyl glycerol tetraethers in soils from two environmental transects in the USA. Organic Geochemistry 59, 49 60.
- Feng, X., D Andrea, W.J., Zhao, C., Xin, S., Zhang, C., Liu, W., 2019. Evaluation of leaf wax D and soil brGDGTs as tools for paleoaltimetry on the southeastern Tibetan Plateau. Chemical Geology 523, 95 106.
- Fick, S.E., Hijmans, R.J., 2017. WorldClim 2: new 1-km spatial resolution climate surfaces for global land areas. International Journal of Climatology 37, 4302–4315.
- Finnegan, S., Bergmann, K., Eiler, J.M., Jones, D.S., Fike, D.A., Eisenman, I., Hughes, N. C., Tripati, A.K., Fischer, W.W., 2011. The magnitude and duration of Late Ordovician-Early Silurian glaciation. Science 331, 903 906.
- Fleming, L.E., Tierney, J.E., 2016. An automated method for the determination of the  $TEX_{86}$  and  $U_{37}^{K'}$  paleotemperature indices. Organic Geochemistry 92, 84–91.
- Gallagher, T.M., Sheldon, N.D., 2016. Combining soil water balance and clumped isotopes to understand the nature and timing of pedogenic carbonate formation. Chemical Geology 435, 79–91.
- Ghosh, P., Adkins, J., Affek, H., Balta, B., Guo, W., Schauble, E.A., Schrag, D., Eiler, J.M., 2006. <sup>13</sup>C <sup>18</sup>O bonds in carbonate minerals: A new kind of paleothermometer. Geochimica et Cosmochimica Acta 70, 1439 1456.
- Gies, H., Hagedorn, F., Lupker, M., Montluçon, D., Haghipour, N., Van Der Voort, T.S., Eglinton, T.I., 2021. Millennial-age glycerol dialkyl glycerol tetraethers (GDGTs) in forested mineral soils: <sup>14</sup>C-based evidence for stabilization of microbial necromass. Biogeosciences 18, 189–205.
- Guo, J., Ma, T., Liu, N., Zhang, X., Hu, H., Ma, W., Wang, Z., Feng, X., Peterse, F., 2022. Soil pH and aridity influence distributions of branched tetraether lipids in grassland soils along an aridity transect. Organic Geochemistry 164, 104347. https://doi.org/ 10.1016/j.orggeochem.2021.104347.
- Halffman, R., Lembrechts, J., Radujkovic, D., De Gruyter, J., Nijs, I., De Jonge, C., 2022. Soil chemistry, temperature and bacterial community composition drive brGDGT distributions along a subarctic elevation gradient. Organic Geochemistry 163, 104346. https://doi.org/10.1016/j.orggeochem.2021.104346.
- Hargreaves, G.H., Samani, Z.A., 1985. Reference crop evapotranspiration from temperature. Applied Engineering in Agriculture 1, 96–99.
- He, Y., Wang, H., Meng, B., Liu, H., Zhou, A., Song, M., Kolpakova, M., Krivonogov, S., Liu, W., Liu, Z., 2020. Appraisal of alkenone- and archaeal ether-based salinity indicators in mid-latitude Asian lakes. Earth and Planetary Science Letters 538, 116236. https://doi.org/10.1016/j.epsl.2020.116236.
- Hopmans, E.C., Weijers, J.W.H., Schefu, E., Herfort, L., Sinninghe Damste, J.S., Schouten, S., 2004. A novel proxy for terrestrial organic matter in sediments based on branched and isoprenoid tetraether lipids. Earth and Planetary Science Letters 224, 107 116.
- Hopmans, E.C., Schouten, S., Sinninghe Damste, J.S., 2016. The effect of improved chromatography on GDGT-based palaeoproxies. Organic Geochemistry 93, 1 6.
- Huguet, C., Hopmans, E.C., Febo-Ayala, W., Thompson, D.H., Sinninghe Damste, J.S., Schouten, S., 2006. An improved method to determine the absolute abundance of glycerol dibiphytanyl glycerol tetraether lipids. Organic Geochemistry 37, 1036 1041.
- Huguet, A., Fosse, C., Metzger, P., Fritsch, E., Derenne, S., 2010. Occurrence and distribution of extractable glycerol dialkyl glycerol tetraethers in podzols. Organic Geochemistry 41, 291 301.
- Huguet, A., Meador, T.B., Laggoun-Defarge, F., Konneke, M., Wu, W., Derenne, S., Hinrichs, K.-U., 2017. Production rates of bacterial tetraether lipids and fatty acids in

- peatland under varying oxygen concentrations. Geochimica et Cosmochimica Acta 203, 103 116.
- Jager, T., 1982. Soils of the Serengeti woodlands. Tanzania, Pudoc Wageningen.
  Kelson, J.R., Huntington, K.W., Schauer, A.J., Saenger, C., Lechler, A.R., 2017. Toward a universal carbonate clumped isotope calibration: Diverse synthesis and preparatory methods suggest a single temperature relationship. Geochimica et Cosmochimica Acta 197. 104 131.
- Kelson, J.R., Huntington, K.W., Breecker, D.O., Burgener, L.K., Gallagher, T.M., Hoke, G. D., Petersen, S.V., 2020. A proxy for all seasons? A synthesis of clumped isotope data from Holocene soil carbonates. Quaternary Science Reviews 234, 106259. https://doi.org/10.1016/j.quascirev.2020.106259.
- Kemp, D.B., Robinson, S.A., Crame, J.A., Francis, J.E., Ineson, J., Whittle, R.J., Bowman, V., O Brien, C., 2014. A cool temperate climate on the Antarctic Peninsula through the latest Cretaceous to early Paleogene. Geology 42, 583–586.
- Kraus, M.J., 1999. Paleosols in clastic sedimentary rocks: their geologic applications. Earth-Science Reviews 47, 41–70.
- Li, J., Pancost, R.D., Naafs, B.D.A., Yang, H., Zhao, C., Xie, S., 2016. Distribution of glycerol dialkyl glycerol tetraether (GDGT) lipids in a hypersaline lake system. Organic Geochemistry 99, 113 124.
- Li, Y., Zhao, S., Pei, H., Qian, S., Zang, J., Dang, X., Yang, H., 2018. Distribution of glycerol dialkyl glycerol tetraethers in surface soils along an altitudinal transect at cold and humid Mountain Changbai: Implications for the reconstruction of paleoaltimetry and paleoclimate. Science China Earth Sciences 61, 925–939.
- Lizama, C., Monteoliva-Sanchez, M., Prado, B., Ramos-Cormenzana, A., Weckesser, J., Campos, V., 2001. Taxonomic study of extreme halophilic archaea isolated from the Salar de Atacama, Chile. Systematic and Applied Microbiology 24, 464–474.
- Lu, H., Liu, W., Yang, H., Wang, H., Liu, Z., Leng, Q., Sun, Y., Zhou, W., An, Z., 2019. 800-kyr land temperature variations modulated by vegetation changes on Chinese Loess Plateau. Nature Communications 10, 1958.
- Menges, J., Huguet, C., Alcaniz, J.M., Fietz, S., Sachse, D., Rosell-Mele, A., 2014. Influence of water availability in the distributions of branched glycerol dialkyl glycerol tetraether in soils of the Iberian Peninsula. Biogeosciences 11, 2571 2581.
- Molnar, P., 2022. Differences between soil and air temperatures: Implications for geological reconstructions of past climate. Geosphere 18, 800–824.
- Naafs, B.D.A., Gallego-Sala, A.V., Inglis, G.N., Pancost, R.D., 2017. Refining the global branched glycerol dialkyl glycerol tetraether (brGDGT) soil temperature calibration. Organic Geochemistry 106, 48–56.
- Naafs, B.D.A., Oliveira, A.S.F., Mulholland, A.J., 2021. Molecular dynamics simulations support the hypothesis that the brGDGT paleothermometer is based on homeoviscous adaptation. Geochimica et Cosmochimica Acta 312, 44 56.
- Norton-griffiths, M., Herlocker, D., Pennycuick, L., 1975. The patterns of rainfall in the Serengeti Ecosystem, Tanzania. African Journal of Ecology 13, 347–374.
- Peaple, M.D., Beverly, E.J., Garza, B., Baker, S., Levin, N.E., Tierney, J.E., Haggi, C., Feakins, S.J., 2021a. Abundances and indices for soil microbial biomarkers (brGDGTs and isoGDGTs) in eleven soil profiles across a Serengeti transect. Pangaea.
- Peaple, M.D., Tierney, J.E., McGee, D., Lowenstein, T.K., Bhattacharya, T., Feakins, S.J., 2021b. Identifying plant wax inputs in lake sediments using machine learning. Organic Geochemistry 156, 104222. https://doi.org/10.1016/j. orgeochem.2021.104222.
- Pei, H., Zhao, S., Yang, H., Xie, S., 2021. Variation of branched tetraethers with soil depth in relation to non-temperature factors: Implications for paleoclimate reconstruction. Chemical Geology 572, 120211. https://doi.org/10.1016/j. chemeo.2021.120211
- Perez-Angel, L.C., Sepúlveda, J., Molnar, P., Montes, C., Rajagopalan, B., Snell, K., Gonzalez-Arango, C., Dildar, N., 2020. Soil and air temperature calibrations using branched GDGTs for the tropical Andes of Colombia: Toward a pan-tropical calibration. Geochemistry, Geophysics, Geosystems 21, e2020GC008941.
- Peterse, F., Kim, J.-H., Schouten, S., Kristensen, D.K., Koç, N., Sinninghe Damste, J.S., 2009. Constraints on the application of the MBT/CBT palaeothermometer at high latitude environments (Svalbard, Norway). Organic Geochemistry 40, 692 699.
- Peterse, F., van der Meer, J., Schouten, S., Weijers, J.W.H., Fierer, N., Jackson, R.B., Kim, J.-H., Sinninghe Damste, J.S., 2012. Revised calibration of the MBT CBT paleotemperature proxy based on branched tetraether membrane lipids in surface soils. Geochimica et Cosmochimica Acta 96, 215–229.
- Peterse, F., Martínez-García, A., Zhou, B., Beets, C.J., Prins, M.A., Zheng, H., Eglinton, T. I., 2014. Molecular records of continental air temperature and monsoon precipitation variability in East Asia spanning the past 130,000 years. Quaternary Science Reviews 83, 76–82.
- Petersen, S.V., Defliese, W.F., Saenger, C., Daeron, M., Huntington, K.W., John, C.M., Kelson, J.R., Bernasconi, S.M., Colman, A.S., Kluge, T., Olack, G.A., Schauer, A.J., Bajnai, D., Bonifacie, M., Breitenbach, S.F.M., Fiebig, J., Fernandez, A.B., Henkes, G. A., Hodell, D., Katz, A., Kele, S., Lohmann, K.C., Passey, B.H., Peral, M.Y., Petrizzo, D.A., Rosenheim, B.E., Tripati, A., Venturelli, R., Young, E.D., Winkelstern, I.Z., 2019. Effects of improved <sup>17</sup>O correction on interlaboratory agreement in clumped isotope calibrations, estimates of mineral-specific offsets, and temperature dependence of acid digestion fractionation. Geochemistry, Geophysics, Geosystems 20, 3495–3519.
- Reed, D.N., Anderson, T.M., Dempewolf, J., Metzger, K., Serneels, S., 2009. The spatial distribution of vegetation types in the Serengeti ecosystem: the influence of rainfall and topographic relief on vegetation patch characteristics. Journal of Biogeography 36, 770, 782
- Schauble, E.A., Ghosh, P., Eiler, J.M., 2006. Preferential formation of <sup>13</sup>C <sup>18</sup>O bonds in carbonate minerals, estimated using first-principles lattice dynamics. Geochimica et Cosmochimica Acta 70, 2510 2529.

- Schouten, S., Hopmans, E.C., Sinninghe Damste, J.S., 2004. The effect of maturity and depositional redox conditions on archaeal tetraether lipid palaeothermometry. Organic Geochemistry 35, 567–571.
- Setia, R., Gottschalk, P., Smith, P., Marschner, P., Baldock, J., Setia, D., Smith, J., 2013. Soil salinity decreases global soil organic carbon stocks. Science of The Total Environment 465, 267–272.
- Sinninghe Damste, J.S., Rijpstra, W.I.C., Hopmans, E.C., Weijers, J.W.H., Foesel, B.U., Overmann, J., Dedysh, S.N., 2011. 13,16-Dimethyl octacosanedioic acid (iso-diabolic acid), a common membrane-spanning lipid of Acidobacteria subdivisions 1 and 3. Applied and Environmental Microbiology 77, 4147–4154.
- Sinninghe Damste, J.S., Rijpstra, W.I.C., Hopmans, E.C., Foesel, B.U., Wüst, P.K., Overmann, J., Tank, M., Bryant, D.A., Dunfield, P.F., Houghton, K., Stott, M.B., Wommack, K.E., 2014. Ether- and ester-bound iso-diabolic acid and other lipids in members of Acidobacteria subdivision 4. Applied and Environmental Microbiology 80, 5207 5218.
- Sinninghe Damste, J.S., Rijpstra, W.I.C., Foesel, B.U., Huber, K.J., Overmann, J., Nakagawa, S., Kim, J.J., Dunfield, P.F., Dedysh, S.N., Villanueva, L., 2018. An overview of the occurrence of ether- and ester-linked iso-diabolic acid membrane lipids in microbial cultures of the Acidobacteria: Implications for brGDGT paleoproxies for temperature and pH. Organic Geochemistry 124, 63 76.
- Tabor, N.J., Myers, T.S., 2015. Paleosols as indicators of paleoenvironment and paleoclimate. Annual Review of Earth and Planetary Sciences 43, 333–361.
- Tierney, J.E., Russell, J.M., Huang, Y., Damsté, J.S.S., Hopmans, E.C., Cohen, A.S., 2008. Northern Hemisphere controls on tropical Southeast African climate during the past 60,000 Years. Science 322, 252 255.
- Turich, C., Freeman, K.H., 2011. Archaeal lipids record paleosalinity in hypersaline systems. Organic Geochemistry 42, 1147 1157.
- Vos, M., Wolf, A.B., Jennings, S.J., Kowalchuk, G.A., 2013. Micro-scale determinants of bacterial diversity in soil. FEMS Microbiology Reviews 37, 936–954.
- Wang, H., Liu, W., Zhang, C.L., Jiang, H., Dong, H., Lu, H., Wang, J., 2013. Assessing the ratio of archaeol to caldarchaeol as a salinity proxy in highland lakes on the northeastern Qinghai-Tibetan Plateau. Organic Geochemistry 54, 69 77.
- Wang, H., Liu, W., Lu, H., Zhang, C., 2017a. Potential degradation effect on paleomoisture proxies based on the relative abundance of archaeal vs. bacterial tetraethers in loess-paleosol sequences on the Chinese Loess Plateau. Quaternary International 436, 173–180.
- Wang, H., Liu, W., He, Y., Zhou, A., Zhao, H., Liu, H., Cao, Y., Hu, J., Meng, B., Jiang, J., Kolpakova, M., Krivonogov, S., Liu, Z., 2021. Salinity-controlled isomerization of lacustrine brGDGTs impacts the associated MBT<sub>SME</sub> terrestrial temperature index. Geochimica et Cosmochimica Acta 305, 33–48.
- Wang, M., Zheng, Z., Man, M., Hu, J., Gao, Q., 2017b. Branched GDGT-based paleotemperature reconstruction of the last 30,000 years in humid monsoon region of Southeast China. Chemical Geology 463, 94 102.
- Weijers, J.W.H., Schouten, S., Hopmans, E.C., Geenevasen, J.A.J., David, O.R.P., Coleman, J.M., Pancost, R.D., Sinninghe Damste, J.S., 2006. Membrane lipids of

- mesophilic anaerobic bacteria thriving in peats have typical archaeal traits. Environmental Microbiology 8, 648–657.
- Weijers, J.W.H., Schouten, S., van den Donker, J.C., Hopmans, E.C., Sinninghe Damste, J. S., 2007. Environmental controls on bacterial tetraether membrane lipid distribution in soils. Geochimica et Cosmochimica Acta 71, 703 713.
- Weijers, J.W.H., Panoto, E., van Bleijswijk, J., Schouten, S., Rijpstra, W.I.C., Balk, M., Stams, A.J.M., Sinninghe Damste, J.S., 2009. Constraints on the biological source(s) of the orphan branched tetraether membrane lipids. Geomicrobiology Journal 26, 402 414.
- Weijers, J.W.H., Wiesenberg, G.L.B., Bol, R., Hopmans, E.C., Pancost, R.D., 2010. Carbon isotopic composition of branched tetraether membrane lipids in soils suggest a rapid turnover and a heterotrophic life style of their source organism(s). Biogeosciences 7, 2959 2973.
- Xie, S., Pancost, R.D., Chen, L., Evershed, R.P., Yang, H., Zhang, K., Huang, J., Xu, Y., 2012. Microbial lipid records of highly alkaline deposits and enhanced aridity associated with significant uplift of the Tibetan Plateau in the Late Miocene. Geology 40, 201–204
- Yamamoto, Y., Ajioka, T., Yamamoto, M., 2016. Climate reconstruction based on GDGT-based proxies in a paleosol sequence in Japan: Postdepositional effect on the estimation of air temperature. Quaternary International 397, 380–391.
- Yang, H., Pancost, R.D., Dang, X., Zhou, X., Evershed, R.P., Xiao, G., Tang, C., Gao, L., Guo, Z., Xie, S., 2014. Correlations between microbial tetraether lipids and environmental variables in Chinese soils: Optimizing the paleo-reconstructions in semi-arid and arid regions. Geochimica et Cosmochimica Acta 126, 49 69.
- Yang, H., Lü, X., Ding, W., Lei, Y., Dang, X., Xie, S., 2015. The 6-methyl branched tetraethers significantly affect the performance of the methylation index (MBT) in soils from an altitudinal transect at Mount Shennongjia. Organic Geochemistry 82, 42, 52
- Zamanian, K., Pustovoytov, K., Kuzyakov, Y., 2016. Pedogenic carbonates: Forms and formation processes. Earth-Science Reviews 157, 1 17.
- Zang, J., Lei, Y., Yang, H., 2018. Distribution of glycerol ethers in Turpan soils: implications for use of GDGT-based proxies in hot and dry regions. Frontiers of Earth Science 12, 862, 876.
- Zech, R., Gao, L., Tarozo, R., Huang, Y., 2012. Branched glycerol dialkyl glycerol tetraethers in Pleistocene loess-paleosol sequences: Three case studies. Organic Geochemistry 53, 38 44.
- Zhang, D., Beverly, E.J., Levin, N.E., Vidal, E., Matia, Y., Feakins, S.J., 2021. Carbon isotopic composition of plant waxes, bulk organics and carbonates from soils of the Serengeti grasslands. Geochimica et Cosmochimica Acta 311, 316–331.
- Zomer, R.J., Bossio, D.A., Trabucco, A., Yuanjie, L., Gupta, D.C., Singh, V.P., 2007. Trees and water: smallholder agroforestry on irrigated lands in Northern India. International Water Management Institute, Colombo, Sri Lanka.
- Zomer, R.J., Trabucco, A., Bossio, D.A., Verchot, L.V., 2008. Climate change mitigation:
   A spatial analysis of global land suitability for clean development mechanism
   afforestation and reforestation. Agriculture, Ecosystems & Environment 126, 67–80.